Nuclear-magnetic-resonance study of crystalline tellurium and selenium

B. Günther and O. Kanert
Institute of Physics, University of Dortmund, 4600 Dortmund 50, West Germany
(Received 21 May 1984; revised manuscipt received 4 September 1984)

Nuclear-magnetic-resonance measurements of ^{125}Te and ^{77}Se have been carried out in single crystals of tellurium and selenium, respectively, between room temperature and the melting point T_m. In particular, both the time evolution of the nuclear magnetization in the laboratory frame as well as in the rotating frame, following both broadband and site-selective excitations, have been investigated in detail. In tellurium, the Zeeman spin-lattice relaxation is determined by three different mechanisms: (1) Below 300 K, spin-lattice relaxation is governed by a two-phonon (Raman) process; (2) in the temperature range between about 300 and 450 K, the influence of conduction electrons overcoming the gap energy of 0.30 eV becomes important; (3) above 450 K, the spin-lattice relaxation is due to mobile charged vacancies. From the high-temperature data, the formation energy of a charged vacancy was found to be 0.66 eV. In selenium, on the other hand, the Zeeman spin-lattice relaxation time is essentially caused by a two-phonon (Raman) process over the entire temperature range. In either system, the phonon-induced spin-lattice relaxation shows the same dependence on the crystal orientation relative to the direction of the external field. For $T \geq 0.74T_m$ in tellurium as well as in selenium, a diffusional contribution to the rotating-frame relaxation rate is observed, arising from fluctuations in the nuclear dipole and chemical shift interaction due to atomic self-diffusion. However, from these data alone the correlation time of atomic motion could be determined only with a relative large error. In contrast, from site-selective excitation experiments the correlation time was extracted directly with a high degree of accuracy without any assumption regarding the nature of the nuclear spin interactions. The observed correlation times are discussed in terms of Mehrer's model for monovacancy diffusion via nearest- and next-nearest-neighbor jumps. Diffusivities in tellurium deduced from this model are in good agreement with the tracer data obtained recently by Mehrer *et al.* In contrast, the observed diffusion coefficients in selenium are about a factor of 20 smaller than the tracer diffusion coefficients measured some years ago by Brätter and Gobrecht.

I. INTRODUCTION

Tellurium as well as isomorphous selenium are elementary semiconductors with very unusual properties.[1] Both systems have a lower crystal symmetry than the "classical" semiconductors germanium and silicon. Furthermore, tellurium and selenium build a relatively soft lattice characterized by low melting points [T_m(Te)=724 K; T_m(Se)=494 K], correspondingly low Debye temperatures [Θ_D(Te)=129 K; Θ_D(Se)=150 K], and low critical shear stresses. However, while tellurium is a low-gap semiconductor [Δ(300 K)=0.32 eV], the band gap of selenium is so large [Δ(300 K)=1.79 eV] that the concentration of intrinsic conduction electrons is negligibly small right up to the melting point.

The NMR properties of both systems are also unique. The low natural abundances of the NMR isotopes ^{125}Te and ^{77}Se of about 7 at.% each result in a small signal which makes an experimental investigation of NMR properties somewhat difficult particularly at higher temperatures. On the other hand, this low abundance also leads to a weak dipole-dipole interaction between the nuclear spins and a corresponding small contribution to the linewidth ($\sim$several hundred Hz). Since both isotopes have a nuclear spin $I=\frac{1}{2}$, disturbing quadrupole interactions do not exist. On the other hand, the high number of orbital electrons is responsible for the fact that the observed chemical-shift interaction is considerably larger than the dipole-dipole interaction. This situation is in contrast to that of materials containing nuclei with low atomic numbers (e.g., ^{1}H or ^{19}F, where the chemical-shift interaction is very small compared to the dipolar interaction).

The crystalline structure of tellurium and selenium can be visualized as a hexagonal arrangement of trigonal helical chains in the $\langle 0001 \rangle$ direction (c axis) as shown in Fig. 1. The atoms within the chains are connected by covalent bonds while the interatomic forces between neighboring chains are more of the van der Waals type. In selenium the covalent character of the binding is more pronounced than in tellurium, as can be inferred from the ratio r of the binding energies between nearest and next-nearest neighbors [see Fig. 1: r(Se)=11.75 and r(Te)=3.1, respectively].

Because of the spiral arrangement of atoms in a 1-2-3 stacking sequence, three types of lattice sites in the unit cell can be distinguished in an NMR experiment. The different orientations of the chemical-shift tensor with respect to the direction of the external magnetic field $\vec{H}_0$ at the different lattice sites lead to a well-separated three-line NMR spectrum of ^{77}Se in single-crystalline selenium[2,3] and of ^{125}Te in single-crystalline tellurium.[4,3] The principal components ($\sigma_0,\sigma_1,\sigma_2,\sigma_3$) of the chemical-shift tensor $\tilde{\sigma}$, written in the usual way as

$$\tilde{\sigma}=\sigma_0\times\mathbb{1}+\begin{bmatrix}\sigma_1 & 0 & 0\\ 0 & \sigma_2 & 0\\ 0 & 0 & \sigma_3\end{bmatrix}, \quad (1)$$

were obtained from the rotation pattern of the NMR spectra[2–4] at $T=77$ K (values in ppm):

^{77}Se: $(\sigma_0=616,\ \sigma_1=-247,\ \sigma_2=-28,\ \sigma_3=275)$,

^{125}Te: $(\sigma_0=886,\ \sigma_1=-620,\ \sigma_2=-570,\ \sigma_3=1190)$.

The angle between the σ_{33} direction and the crystallographic c axis is remarkably smaller in selenium (11°) than in tellurium (47°), indicating the more covalent character of the nearest-neighbor binding in selenium compared to tellurium. The observed chemical-shift tensors have been interpreted theoretically by Bensoussan[5] in a molecular model involving sp^3 hybridization of the valence-electron wave function. Because of the crystal symmetry, for $\vec{H}_0$ parallel to the chain axis c, the three NMR lines collapse into a single line.

In tellurium, the NMR spectrum was shown to be shifted with temperature due to the temperature dependence of the Knight shift K in semiconductors given by the relation[6]

$$K=\text{const}\times\sqrt{T}\,\exp(-\Delta/2kT)\,. \quad (2)$$

Because of the large difference in the gap energies Δ (see above), the Knight shift is unobservable in selenium. Nevertheless, a small additional shift of the ^{77}Se spectrum, proportional to temperature, can be observed (see Sec. III).

Up to now, relatively little nuclear-spin-relaxation data of crystalline tellurium and selenium have been published in the literature. Initial Zeeman spin-lattice relaxation time (T_1) measurements in tellurium were reported in the low-temperature range 40–300 K by Koma *et al.*[7] Neither electronic nor diffusional effects are found at these low temperatures, and T_1 appears to be determined by a two-phonon (Raman) process. More recently, Selbach *et al.*[6] extended the temperature range and demonstrated clearly that, above room temperature, a second relaxation mechanism becomes important. They showed that this second mechanism arises from the creation of intrinsic conduction electrons. Hence, in the temperature range 40–400 K the corresponding total relaxation rate in tellurium obeys the theoretically predicted equation

$$\frac{1}{T_1}=\left.\frac{1}{T_1}\right|_{\text{ph}}+\left.\frac{1}{T_1}\right|_{e}=a_1T^2+a_2T^2\exp\left[-\frac{\Delta}{2kT}\right], \quad (3)$$

with the experimentally determined parameters[8] (with c axis parallel to $\vec{H}_0$)

$$a_1=0.55\times10^{-6}\ \text{s}^{-1}\text{K}^{-2}$$

and

$$a_2=2.64\times10^{-5}\ \text{s}^{-1}\text{K}^{-2}\,.$$

In contrast, the Zeeman spin-lattice relaxation rate in selenium was found to be governed up to the melting point mainly by two-phonon-induced electronic fluctuations, leading to the following relationship,[9,10]

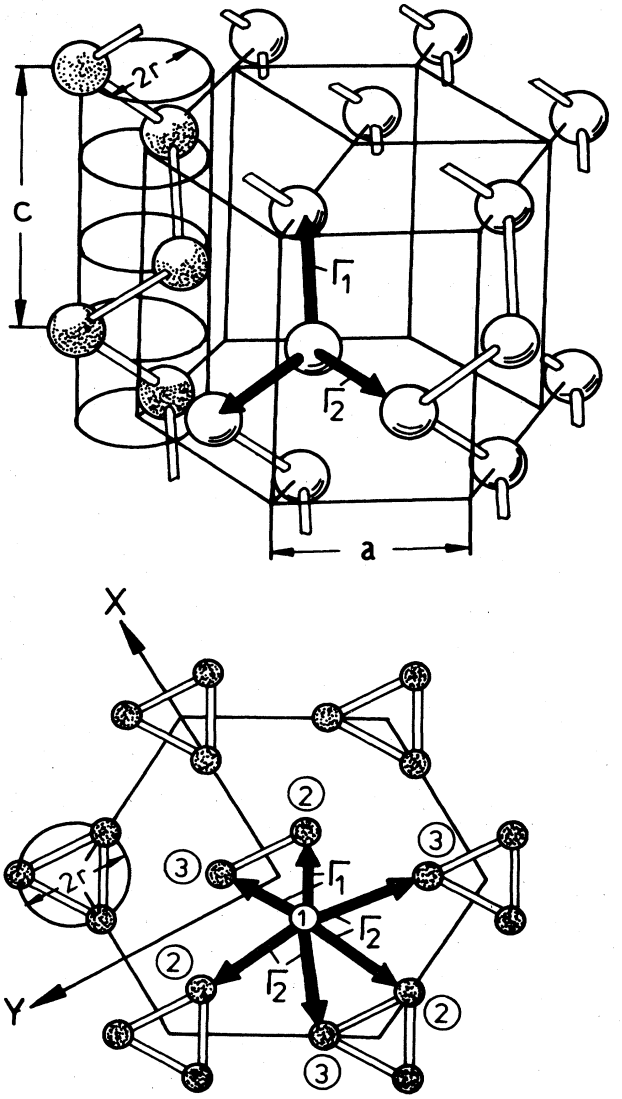

FIG. 1. Crystal structure of tellurium and selenium consisting of spiral chains in c direction arranged in a hexagonal lattice (top). In the bottom half, a view along the c axis illustrates the hexagonal arrangement of the triangular spiral chains. The arrows indicate the nearest (Γ_1) and next-nearest (Γ_2) atomic jumps of the 1V-1N,2N self-diffusion model (Ref. 13).

$$\frac{1}{T_1}=\left.\frac{1}{T_1}\right|_{\text{ph}}=a_1T^2\,, \quad (4)$$

with

$$a_1=2.59\times10^{-8}\ \text{s}^{-1}\text{K}^{-2}\ (c\text{ axis parallel to }\vec{H}_0)\,.$$

By means of radioactive-tracer techniques, atomic self-diffusion in crystalline tellurium was first investigated by Ghoshtagore,[11] and in crystalline selenium by Brätter and Gobrecht.[12] Mehrer has presented a comprehensive theory about the diffusion kinetics and correlation factors in tellurium and selenium.[13] His calculations are based on motion of single vacancies between nearest and next-

nearest lattice sites corresponding to atomic jumps within and between the chains (see Fig. 1). Very recently, Werner *et al.* have very carefully repeated Ghoshtagore's tracer measurements using tellurium single crystals of excellent quality.[14] They obtained diffusion coefficients about a factor of 5 smaller than that previously obtained by Ghoshtagore. Furthermore, their data agree with the diffusion model introduced by Mehrer.[13]

In earlier work[10,15] we demonstrated that atomic motions in tellurium as well as in selenium can be observed very sensitively with a special NMR technique, namely the nonexponential evolution of the nuclear magnetization after site-selective excitation caused by a magnetization transfer arising from atomic jumps. Since then, the theory underlying site-selective experiments have been published in the literature.[8,16–18] Furthermore, in contrast to "classical" nuclear-spin-relaxation experiments the correlation time of the atomic jumps could be obtained directly from such site-selective experiments without any further assumptions regarding nuclear spin interactions.

In the present paper a comprehensive experimental investigation is presented of the NMR behavior of crystalline tellurium and selenium between room temperature and the melting point. In particular, this paper deals with different mechanisms responsible for the evolution of the nuclear spin magnetization observed in classical T_1 and $T_{1\rho}$ experiments as well as in site-selective experiments. Furthermore, correlation times for atomic diffusion are extracted from the NMR measurements and compared with tracer data obtained from the literature. For selenium, atomic jump times of about 10^4 sec (i.e., diffusion coefficients down to about 10^{-19} cm^2/sec) have been observed.

II. EXPERIMENTAL DETAILS

The nuclear-magnetic-resonance measurements were carried out on single crystals of a typical size of about $3\times3\times10$ mm^3 obtained from several sources. The tellurium single crystals were made at the Institute of Physics of the University of Würzburg, whereas the selenium single crystals were produced at the Institute of Physics of the University of Marburg. Because of both the fairly high vapor pressure of Te and the danger of contamination by oxygen, the tellurium crystals were Czochralski-grown in a hydrogen atmosphere using 99.999%-purity tellurium as starting material. The hole concentration at 77 K was 2×10^{13} cm^{-3}. The selenium single crystals were grown from the vapor phase using a 99.999%-purity selenium melt doped with about 0.1 at. % Tl in order to reduce the viscosity of the melt. The total content of impurities (except the concentration of Tl in the selenium crystals) in all the crystals was lower than 10 ppm. The samples were placed in quartz tubes which were flushed with dry argon gas and sealed with gas-tight high-temperature cement.

The specimen under investigation was mounted on a goniometer inside a high-temperature NMR probe containing a single platinum NMR coil capable of operating between room temperature and 900 K. Temperatures were stabilized with a feedback system within ±0.2% over the temperature range investigated. Sample temperatures were measured with a Philips Chromel-Alumel thermocouple which was calibrated against the melting points of 99.999%-purity tellurium and 99.999%-purity selenium. The overall accuracy of the temperature determination was about ±1 K. The high-pressure experiments at room temperature were performed with use of a commercial high-pressure system [Nova Swiss/Effretikon (Switzerland)] using argon as the pressurizing gas. A maximum pressure of about 2.5 kbar could be attained. The rf coil inside the high-pressure NMR probe built from copper-beryllium was wound directly around the sample.

The nuclear magnetic resonance of ^{125}Te and ^{77}Se was observed with a modified Bruker SXP 4-100 coherent pulsed NMR spectrometer including an on-line data-processing system in order to improve the signal-to-noise ratio by signal averaging and to evaluate the experimental data. The NMR measurements were made at various magnetic fields in the range between 1.4 and 6.3 T. The NMR spectra were obtained from Fourier transformation of the off-resonance free induction decay following a $\pi/2$ pulse. The positions of the ^{125}Te spectra and ^{77}Se spectra were referred to solid $TeCl_2$ and to an aqueous solution of H_2SeO_3, respectively. We used both a π-($\pi/2$) pulse sequence and a saturation pulse comb a time τ prior to the $\pi/2$ reading pulse to measure the time evolution of the nuclear magnetization in the laboratory frame. We applied a spin-locking technique (consisting of a strong $\pi/2$ pulse followed by a long locking pulse of strength H_1 shifted in rf phase by $\pi/2$ with respect to the first pulse) to observe the evolution of the magnetization in the rotating frame. By varying the crystal orientation and thus the separation of the NMR lines, the time evolution of the magnetization of each line could be observed separately either after a complete saturation of the total spectrum or after a site-selective excitation of a single line.

III. NUCLEAR-MAGNETIC-RESONANCE SPECTRA

The nuclear spin Hamiltonian which describes the spectrum of ^{125}Te in crystalline tellurium and of ^{77}Se in crystalline selenium can be written as

$$\hat{H}=\hat{H}_Z+\hat{H}_D+\hat{H}_C+\hat{H}_F\ . \tag{5}$$

Here, the Zeeman term $\hat{H}_Z$ describes the interaction of the spin system with the external magnetic field $\vec{\mathrm{H}}_0$, $\vec{\mathrm{H}}_D$ denotes the magnetic dipole-dipole interaction, $\hat{H}_C$ is the chemical shift Hamiltonian, and $\hat{H}_F$ is the Fermi contact operator which describes the interaction between the nuclear spins and conduction electrons. (See Abragam[19] for detailed expressions for these different operators.) The operator $\hat{H}_C$ which is responsible for the three-line spectrum in tellurium and selenium can be related to the shift tensor $\tilde{\sigma}$ as follows:

$$\hat{H}_C=-\gamma h\vec{\mathrm{H}}_0 N[\sigma_0+\tfrac{1}{3}(\tilde{\sigma}_A^{(1)}+\tilde{\sigma}_A^{(2)}+\tilde{\sigma}_A^{(3)})]\hat{I}\ , \tag{6}$$

where N is the number of spins with spin operator $\hat{I}$ and gyromagnetic ratio γ, $\sigma_0=\frac{1}{3}\,\mathrm{tr}\tilde{\sigma}$, and $\tilde{\sigma}_A^{(i)}$ is the anisotropic traceless part of $\tilde{\sigma}$ at site i ($i=1,2,3$) given by

$\tilde{\sigma}_A = \frac{1}{2}(\tilde{\sigma} + \tilde{\sigma}^T) - \sigma_0$, where $\tilde{\sigma}^T$ is the transpose of $\tilde{\sigma}$.

As shown in Fig. 2, the width of the three lines of the NMR spectra are inhomogeneously broadened by misfits $\delta\tilde{\sigma}_A$ of the anisotropic part $\tilde{\sigma}_A$. The misfit $\delta\tilde{\sigma}_A$ is due to lattice imperfections, probably dislocations. Hence, according to Eq. (6) the inhomogeneous broadening function $g_C(\omega)$ of a given line can be written as

$$g_C(\omega) = \gamma H_0 g(\delta\sigma_A^{zz}) , \tag{7}$$

where the function $g(\delta\sigma_A^{zz})$ describes the distribution of the components $\delta\sigma_A^{zz}$ of the misfit tensors $\delta\tilde{\sigma}_A$ in the direction of the applied magnetic field $\vec{H}_0$. Assuming, as a first approximation, Gaussian functions for $g_C(\omega)$ as well as for the field-independent dipolar broadening function $g_D(\omega)$ determined by the operator $\hat{H}_D$ in Eq. (6), the total half-width $\delta\nu$ of the line may be expressed as

$$\delta\nu = (\delta\nu_D^2 + cH_0^2)^{1/2} . \tag{8}$$

Here $\delta\nu_D$ denotes the width of $g_D(\omega)$ and the constant c is proportional to the concentration of defects, which in turn are responsible for the inhomogeneous line broadening. The experimental data in Fig. 2 are fitted by Eq. (8) using $\delta\nu_D$ and c as fit parameters. The experimental values of $\delta\nu_D$ given by the ordinate sections of Fig. 2 [$\delta\nu_D$(Te)=360 Hz and $\delta\nu_D$(Se)=130 Hz] agree roughly with the theoretical dipolar widths calculated by Van Vleck's second-moment formula[20] by taking into account the rare natural abundance of the isotopes having a magnetic moment.[21]

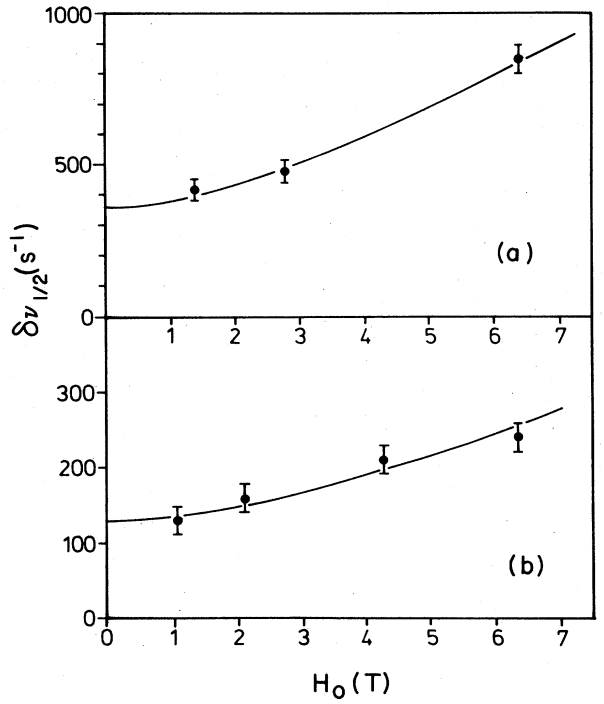

FIG. 2. Magnetic field dependence of the half-width $\delta\nu_{1/2}$ of (a) the ^{125}Te NMR spectrum in tellurium and (b) the ^{77}Se NMR spectrum in selenium at room temperature (angle between crystallographic c axis and the magnetic field direction is $\theta = 50°$). The solid lines are fits based on Eq. (8).

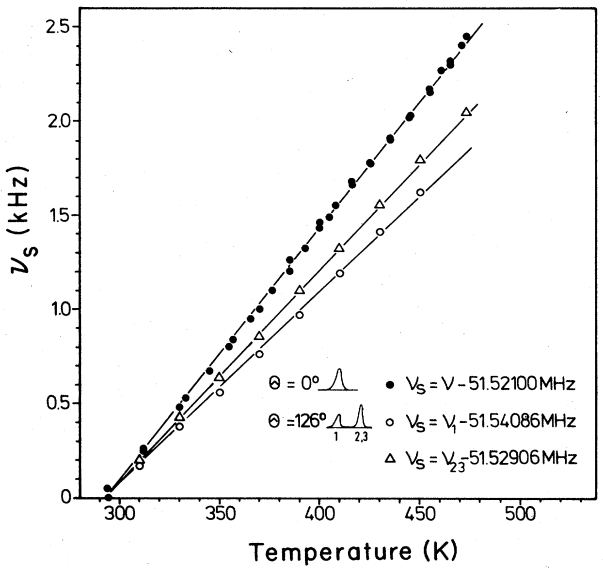

FIG. 3. Temperature shift of the several ^{77}Se resonance frequencies for two different crystal orientations in the magnetic field ($\theta = 0°$ and 126°, respectively, with X axis perpendicular to $\vec{H}_0$) referred to the corresponding frequencies at room temperature. Magnetic field strength $H_0 = 6.3$ T.

As shown previously,[6] the number of electrons in the valence band of tellurium gives rise to a temperature-dependent Knight shift K of the ^{125}Te spectrum described by Eq. (2). This effect is unobservable in the ^{77}Se spectrum of selenium because of the large energy gap Δ of selenium. Nevertheless, as depicted in Fig. 3, between room temperature and the melting point the ^{77}Se lines are linearly shifted with increasing temperature, the shift depending slightly on the crystal orientation. Hence, one concludes from the data that the chemical-shift interaction probably depends on temperature. Additional measurements of the orientation dependence of the shift have shown that both the isotropic part σ_0 and the anisotropic part $\sigma_1, \sigma_2, \sigma_3$ change slightly with varying temperature (see Table I). The observed temperature dependence of the chemical-shift interaction is probably caused by the thermal lattice expansion but, to the best of our knowledge up to now, a more precise theory of this effect does not exist.

TABLE I. Principal components σ_i (in ppm) of the chemical-shift tensor of ^{77}Se in crystalline selenium for three different temperatures.

	77 K[a]	290 K	480 K
σ_0	615.7	509.5	470.0
σ_1	−247.1	−234	−221.1
σ_2	−28.1	−25	−32.5
σ_3	275.2	259	253.6

[a] Reference 4.

IV. NUCLEAR SPIN RELAXATION

A. Single-line experiments

For an external field $\vec{H}_0$ parallel to the chain direction (c axis) of the crystal ($\theta=0°$) the three lines of the NMR spectra collapse and a single-line spectrum is observed. In such an orientation, spin-lattice relaxation times T_1 and $T_{1\rho}$ were measured in tellurium and selenium from room temperature to the melting point.

1. Tellurium

A logarithmic plot of the experimental T_1 and $T_{1\rho}$ data of ^{125}Te in tellurium versus reciprocal temperature is shown in Fig. 4. As described by Eq. (3), the temperature variation of the relaxation rate $1/T_1$ below 400 K is determined by the interaction of the nuclear spins with phonons and conduction electrons. Above 400 K the slope of $1/T_1$ shows an additional increase, indicating that a third relaxation mechanism is activated. Hence, by extending Eq. (3) the total relaxation rate $1/T_1$ can be written as

$$\frac{1}{T_1}=a_1T^2+a_2T^2\exp\left[-\frac{\Delta}{2kT}\right]+\left.\frac{1}{T_1}\right|_{\mathrm{CV}}, \tag{9}$$

where $1/T_1\,|_{\mathrm{CV}}$ denotes the relaxation rate of the third mechanism. The strong Arrhenius-type temperature dependence of $1/T_1\,|_{\mathrm{CV}}$ and its weak dependence on the magnetic field strength suggests the following relaxation mechanism: If a bond within a tellurium chain is broken by formation of a vacancy, an electronic acceptor state is created, since the free tellurium bonds at the chain end tend to be saturated by free electrons.

Hörstel and Kretschmar[22] have investigated the temperature dependence of the acceptor concentration by measuring the Hall coefficient after quenching and annealing of tellurium single crystals. They concluded that thermally created charged vacancies with a formation energy of (0.8±0.1) eV are indeed the origin of the acceptor states. Hence, analogous to conduction-electron-induced nuclear spin relaxation, the relaxation rate $1/T_1\,|_{\mathrm{CV}}$ may be attributed to the effect of charged vacancies. According to Hörstel and Kretschmar,[22] a one-electron acceptor state is created if a bond within a tellurium chain is broken by formation of a vacancy. They derived this model by comparing the Te_2 binding energy with the formation energy of a neutral vacancy. Unfortunately, there is not yet any direct experimental confirmation of this model. If the electronic correlation time τ_e of a charged vacancy is assumed to be small compared to the correlation time τ_m of the vacancy motion, $1/T_1\,|_{\mathrm{CV}}$ can be expressed as follows:[23]

$$\left.\frac{1}{T_1}\right|_{\mathrm{CV}}=\tfrac{9}{4}\gamma^2\gamma_e^2\hbar^2S(S+1)f\tau_eC_{\mathrm{CV}}\,. \tag{10}$$

Here, γ_e and S are the electronic gyromagnetic ratio and spin, respectively. f denotes a lattice sum and C_{CV} is the concentration of thermally created charged vacancies,

$$C_{\mathrm{CV}}(T)=C_0\exp\left[-\frac{E_f^{\mathrm{CV}}}{kT}\right], \tag{11}$$

with E_f^{CV} being the formation energy of a vacancy. Equation (10) is derived using the condition that $1/\tau_e$ is large compared to the electronic Larmor frequency $\omega_e=\gamma_eH_0$, which follows from the experimental observation that $1/T_1\,|_{\mathrm{CV}}$ is independent of the magnetic field strength H_0 (see also Fig. 4). According to Abragam and Bleaney,[24] the electronic correlation time τ_e is determined by three processes: the Orbach process, the single-phonon (direct), and the two-phonon (Raman) process. For temperatures above the Debye temperature, τ_e is governed by the Raman process leading to $\tau_e\sim T^{-2}$. Then, Eq. (10) may be written as

$$\left.\frac{1}{T_1}\right|_{\mathrm{CV}}T^2=b_0\exp\left[-\frac{E_f^{\mathrm{CV}}}{kT}\right], \tag{12}$$

with $b_0=$const.

To experimentally obtain the relaxation rate $1/T_1\,|_{\mathrm{CV}}$, one must subtract the phonon- and conduction-electron-induced contributions given by Eq. (3) from the T_1 data of Fig. 4. Figure 5 shows that the experimental data thus obtained obey a temperature law predicted by Eq. (12) over more than five decades. The slope of the curve leads to a formation energy E_f^{CV} of (0.66±0.01) eV. This result is in fairly good agreement with the value estimated by Hörstel and Kretschmar in view of the relatively large experimental errors given by these authors.[22] Furthermore, the experimental value of b_0 was found to be $b_0=4.42\times10^{12}\,\mathrm{s^{-1}K^2}$.

To the best of our knowledge, the interaction mechanism of the phonon-induced contribution $1/T_1\,|_{\mathrm{ph}}$ is not understood clearly. A phonon-induced fluctuation of the chemical-shift interaction would lead to $1/T_1\,|_{\mathrm{ph}}\propto H_0^2$,[19]

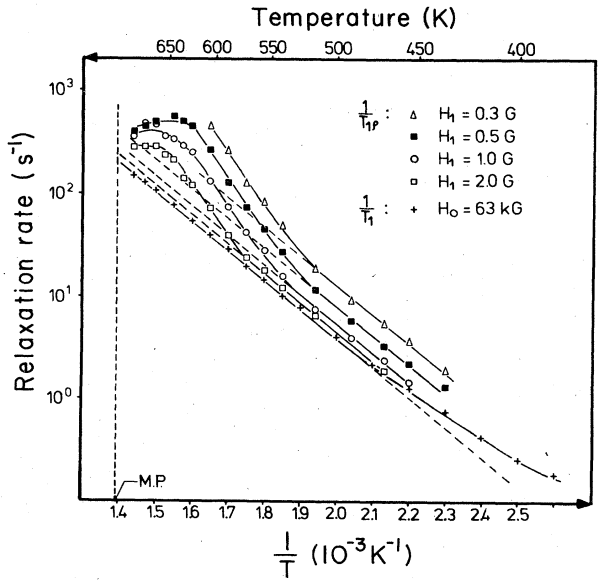

FIG. 4. Temperature dependence of the ^{125}Te spin-lattice relaxation rates $1/T_1$ and $1/T_{1\rho}$ in a tellurium single crystal for c axis parallel to the magnetic field ($\theta=0°$).

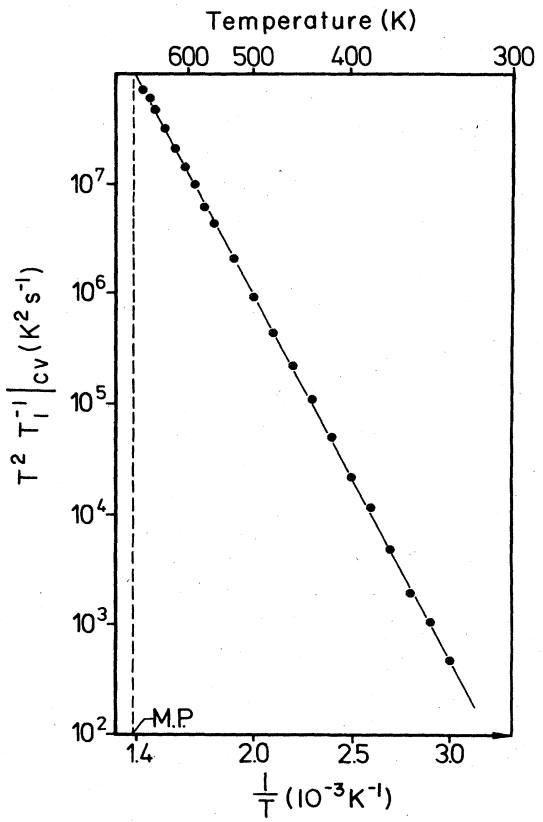

FIG. 5. Arrhenius plot of the charged-vacancy-induced part of the relaxation rate $1/T_1 \mid_{CV}$ multiplied by the square of temperature of ^{125}Te in tellurium. The straight line confirms Eq. (12) with an activation energy of 0.66 eV for the formation of charged vacancies.

but the experimental data of $1/T_1 \mid_{ph}$ were found to be *independent* of the magnetic field strength. Koma *et al.*[7] proposed for the relaxation mechanism a second-order phonon-electron interaction which scatters electrons into the conduction band. According to Koma's calculation based on this model, $T_1 \mid_{ph}$ should be proportional to Δ^4/T^2. On the other hand, as shown by Kosichkin,[25] a hydrostatic pressure p drastically affects the magnitude of the band gap Δ of tellurium according to the relation $\Delta(p)=\Delta(0)\exp(-\alpha p)$, with $\alpha=0.063$ kbar^{-1}. Thus, one expects to see an analogous pressure dependence of $T_1 \mid_{ph}$ given by

$$T_1(p) \mid_{ph} = T_1(0) \mid_{ph} \exp(-4\alpha p) \; . \tag{13}$$

However, contrary to that proposal, the experimental data of $T_1 \mid_{ph}$ depicted in Fig. 6 are found to be independent of the applied hydrostatic pressure p. The measurements have been performed at $T=290$ K, where the spin-lattice relaxation is governed mainly by the phonon-induced contribution, while the other two contributions are only about 10% of the total relaxation rate [see Eqs. (9) and (12)]. The conclusion must be drawn that neither chemical-shift fluctuations nor phonon-created conduction electrons are accountable for the phonon-induced relaxation. In our opinion, the relaxation mechanism is due probably to a two-phonon- (Raman) induced fluctuation of nuclear-

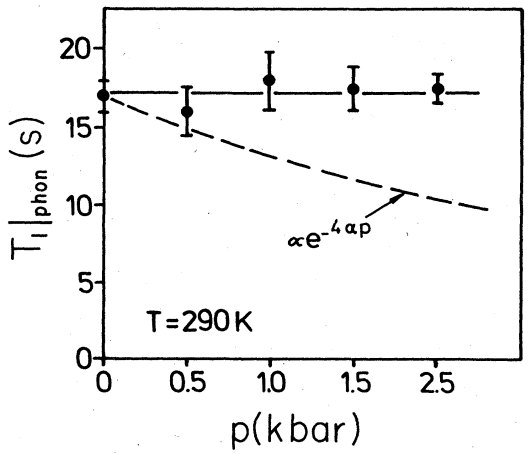

FIG. 6. Phonon-induced part of the relaxation time, $T_1 \mid_{ph}$, of ^{125}Te in tellurium vs hydrostatic pressure. The dashed line represents the behavior as expected from Koma's model (Ref. 17) [see Eq. (13)].

spin—electron-orbit coupling. Indeed, such a mechanism is expected to be independent of the magnitude of H_0 and of Δ, but leads to the experimentally observed T^2 law above Debye temperature.

Additional measurements of $T_1 \mid_{ph}$ as a function of the crystal orientation with respect to $\vec{H}_0$ show a pronounced orientation dependence of the coefficient a_1 in Eq. (3) [and also in Eq. (4) in the case of selenium], which can be expressed as

$$a_1 = a + b\cos[2(\theta+\phi_0)] \; . \tag{14}$$

Values of the coefficients a, b, and ϕ_0 are given in Table II for one of the NMR lines of the ^{125}Te and ^{77}Se spectrum, in which the crystallographic X axis is the axis of rotation (see Fig. 1). θ denotes the angle between $\vec{H}_0$ and the c axis. The large orientation dependence of $T_1 \mid_{ph}$ reflects the low crystal symmetry of the lattice structure of tellurium and selenium.

As depicted in Fig. 4, contrary to the monotonic behavior of $1/T_1$, the rotating-frame relaxation rate $1/T_{1\rho}$ shows a weak additional BPP-like (BPP denotes Bloembergen-Purcell-Pound) contribution above 550 K due to translational atomic diffusion. The field dependence of the "background" relaxation rate $1/T_{1\rho} \mid_b$ characterized by the dashed lines in Fig. 4 follows the relationship

$$T_{1\rho} \mid_b = T_1 \frac{H_1^2 + H_{L\rho}^2}{H_1^2 + \delta H_{L\rho}^2} \; , \tag{15}$$

TABLE II. Values of a and b (in 10^{-8} s^{-1}K^{-2}), and ϕ_0 in Eq. (14) for ^{125}Te and ^{77}Se nuclei on lattice sites of type 1 (see Fig. 1), and for the crystallographic X axis ($\perp\vec{H}_0$) being the axis of rotation.

	a	b	ϕ_0 (deg)
Te	60.6	10.7	59
Se	3.98	1.6	105

which is valid for a "fast" relaxation process, i.e., $\omega_e\tau_e \ll 1$. τ_e is the electronic correlation time of the charged vacancies and $H_{L\rho}$ is the total local field (dipolar and chemical-shift-broadened) in the rotating frame. A fit of the experimental data using Eq. (15) leads to $\delta=3.3$ and $H_{L\rho}=0.36$ G.

The diffusion-induced part of the rotating-frame relaxation rate, $1/T_{1\rho}\,|_{\text{diff}}$, obtained by subtracting the "background" rate $1/T_{1\rho}\,|_b$, is shown in Fig. 7 as a function of the inverse temperature. At all temperatures the differences between $1/T_{1\rho}$ and $1/T_{1\rho}\,|_b$ (dashed lines) are fairly small, which leads to substantial error bars for $1/T_{1\rho}\,|_{\text{diff}}$. Since these large error bars are greater than the difference between analogous expressions[8] obtained with more sophisticated theories, such as those of Torrey,[26] Wolf,[27] and Sholl and Barton,[28] we found it sufficient to analyze the data by means of simple BPP expressions. $1/T_{1\rho}\,|_{\text{diff}}$ is assumed to be due to diffusion-induced fluctuations both of the dipolar interaction and of the chemical-shift misfits $\delta\tilde{\sigma}_A$. Then, taking into account the pair-correlated structure of the dipolar fluctuation and the autocorrelated structure of the chemical shift fluctuation, $1/T_{1\rho}\,|_{\text{diff}}$ can be expressed in the BPP approximation as[8]

$$\left.\frac{1}{T_{1\rho}}\right|_{\text{diff}}=\gamma^2H_{D\rho}^2\frac{\tau_D}{1+(2\omega_\rho\tau_D)^2}+\gamma^2H_{c\rho}^2\frac{\tau}{1+(\omega_\rho\tau)^2}\ . \qquad (16)$$

Here, the correlation time τ denotes the correlated mean time between two consecutive atomic jumps, and $H_{c\rho}^2$ is the fluctuating part of the mean-squared chemical-shift broadening in the rotating frame. Its approximate dependence on the mean-squared average of $\delta\sigma_A^{zz}$ [see Eq. (7)] is given by $H_{c\rho}^2\simeq H_0^2\langle(\delta\sigma_A^{zz})^2\rangle$. Also, $\omega_\rho=\gamma(H_1^2+H_{L\rho}^2)^{1/2}$ is the effective strength of the locking field. It should be noted that the second part of Eq. (16) is valid for $(H_1\sigma_A^{zz})\ll[H_0\langle(\delta\sigma_A^{zz})^2\rangle^{1/2}]$. Since the dipolar correlation time τ_D is related to τ by $\tau_D=\tau/2$,[27] Eq. (16) may be simplified as

$$\left.\frac{1}{T_{1\rho}}\right|_{\text{diff}}=\gamma^2H_{L\rho}^2\,|_{\text{dyn}}\frac{\tau}{1+(\omega_\rho\tau)^2}\ , \qquad (17)$$

with $H_{L\rho}^2\,|_{\text{dyn}}=H_{D\rho}^2/2+H_{c\rho}^2$ denoting the mean-squared change of the local field in the rotating frame on atom experiences due to a single correlated jump process.

The experimental data of Fig. 7 could be fitted by means of Eq. (17) with a single thermally activated atomic jump frequency,

$$\frac{1}{\tau}=(2.8\pm1.4)\times10^{15}\exp\{[-(1.47\pm0.05)\text{ eV}]/kT\}\ \text{s}^{-1}\ ,$$

using $H_{L\rho}=(0.37\pm0.04)$ G and $H_{L\rho}\,|_{\text{dyn}}=(0.26\pm0.02)$ G as best-fit parameters. The solid lines in Fig. 7 demonstrate the quality of the fit procedure. The total local field $H_{L\rho}$ thus measured is in good agreement with the value of 0.36 G determined from the background relaxation formula, Eq. (15).

In principle, from the temperature dependence of the correlation time τ given above, the diffusion coefficient D can be calculated as a function of temperature by means of an Einstein-Smoluchovsky relation, as formulated by Mehrer,[13] for the lattice structure of tellurium [see Eq. (27)]. But, as shown in Sec. IV B, site-selective excitation of a single line of the NMR spectrum turns out to be a much more precise tool for measuring τ. Hence, such precisely determined atomic jump times will be used to obtain self-diffusion coefficients.

2. *Selenium*

In a manner analogous to that of Fig. 4, the temperature dependence of the ^{77}Se spin-lattice relaxation rates $1/T_1$ and $1/T_{1\rho}$ in selenium are depicted in Fig. 8 for $\vec{H}_0$

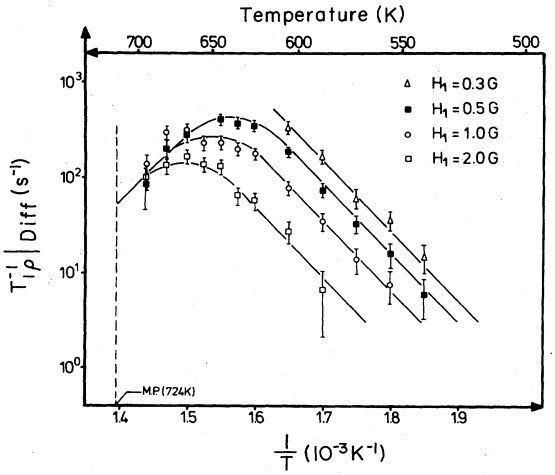

FIG. 7. Diffusion-induced contribution to the relaxation rate $1/T_{1\rho}$ in tellurium vs inverse temperature as obtained from Fig. 4. The solid lines are least-squares fits to the data based on Eq. (17) (see text).

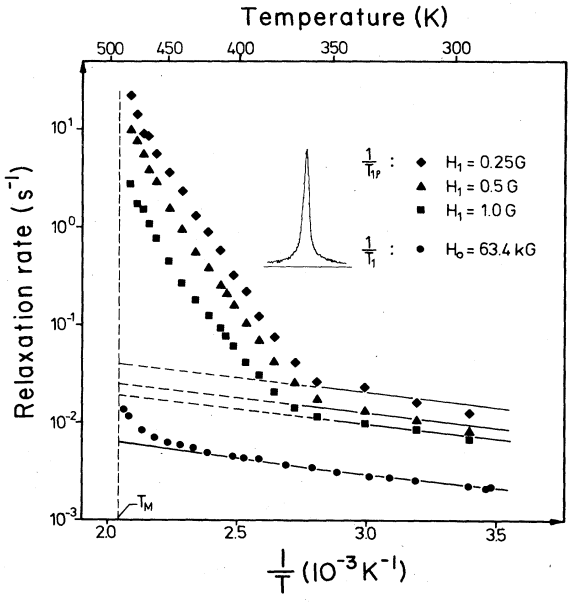

FIG. 8. Temperature dependence of the ^{77}Se spin-lattice relaxation rates $1/T_1$ and $1/T_{1\rho}$ in a selenium single crystal for a single-line orientation of the crystal (c axis parallel to the magnetic field direction; $\theta=0°$).

aligned parallel to the crystallographic c axis (single-line orientation). In contrast to the relaxation behavior of ^{125}Te in tellurium, which is governed by three relaxation mechanisms [see Eq. (9)], the Zeeman relaxation rate $1/T_1$ of ^{77}Se in selenium in the entire temperature region is determined essentially by a single relaxation process, namely a two-phonon process described by Eq. (4). As in the case of tellurium, $1/T_1 \mid_{\rm ph}$ depends on the crystal orientation with respect to $\vec{H}_0$, as seen in Eq. (14), where the values of the coefficients a and b found experimentally are presented in Table II. The solid line in Fig. 8 fitted to the T_1 data is obtained from Eqs. (4) and (14) for $\theta=0°$. Likewise, the strength of this relaxation process was found to be *independent* of the magnitude of H_0 (i.e., the relaxation mechanism does not deal with phonon-induced chemical-shift fluctuations). According to Koma's model,[7] the ratio of the phonon-assisted relaxation times of ^{77}Se in selenium and ^{125}Te in tellurium should be equal to $[\Delta(\mathrm{Se})/\Delta(\mathrm{Te})]^4 \doteq 885$, while the experimental data lead to a ratio of only about 15 (see Table II). This discrepancy is further evidence that Koma's theory is not able to explain the phonon-induced relaxation mechanisms in tellurium and in selenium.

Above 450 K, a very small additional increase of the relaxation rate $1/T_1$ is observed with increasing temperature, indicating that a second relaxation mechanism is activated. The corresponding additional relaxation rate is caused by translational atomic jumps. As expected from general relaxation behavior, the strength of this relaxation process should increase with decreasing field strength [see Eq. (17)]. Indeed, this behavior is demonstrated in Fig. 8, where the relaxation rates in a weak rotating field H_1 show a sharp additional increase above 370 K due to atomic motion. In principle, it is possible to extract the atomic jump frequencies $1/\tau$ from these measurements using Eq. (17) in analogy to the analysis of the ^{125}Te relaxation data in tellurium shown in Fig. 7. However, contrary to the $T_{1\rho}$ data of ^{125}Te, the $T_{1\rho}$ data of ^{77}Se show a monotonic temperature dependence and a relaxation-rate maximum does not occur. Hence, a four-parameter fit of these data by means of Eq. (17) cannot be performed successfully; only the activation energy E_A of the thermally activated jump process can be estimated from the slope of the motion-induced contribution to the relaxation rate, $1/T_{1\rho} \mid_{\rm diff}$, obtained by subtracting the phonon-induced rates (dashed lines) from the measured relaxation rates. According to Eq. (17), in the low-temperature region in which $\omega_\rho\tau \gg 1$, the relaxation rate $1/T_{1\rho} \mid_{\rm diff}$ is proportional to $1/\tau(T) \propto \exp(-E_A/kT)$. From an Arrhenius representation of $1/T_{1\rho} \mid_{\rm diff}$ one finds $E_A \simeq 0.9$ eV, which agrees roughly with the results of the more precise site-selective excitation experiments discussed in the next section.

Obviously, below 350 K the rotating-frame relaxation rate $1/T_{1\rho}$, which has been shown to be dominated by phonon-induced fluctuations in this temperature range, does not approach the Zeeman relaxation rate $1/T_1$ for locking fields $H_1 \gg H_{L\rho}$, as expected from Eq. (15). The discrepancy may be probably explained by an orientation dependence of $T_{1\rho}$ with respect to the external field $\vec{H}_0$, which is different to the orientation dependence of T_1.

B. Site-selective excitation

As mentioned in the Introduction, site-selective excitation has been shown to be a very sensitive technique for the investigation of ultraslow atomic motions in solids. This technique has an advantage in not depending on an independent determination of the type or strength of the nuclear spin interactions, in contrast to ordinary nuclear-spin-relaxation experiments, which are governed by relations of the form of Eq. (17).[15,8] This technique can be applied to crystalline solids where the different lines of the NMR spectrum can be associated with corresponding nonequivalent lattice sites in the crystallographic unit cell.

There will be a single background spin-lattice relaxation rate $1/T_1$ for all the lines caused, for instance, by spin-phonon scattering processes. In addition, hopping of the nuclei via atomic jumps between the lattice sites gives rise to a transfer of nuclear magnetization between the corresponding NMR lines, which, in turn, may be regarded as a cross-relaxation process. Under site-selective excitation of one of the lines of the NMR spectrum, nonexponential time evolution of the z magnetization generally occurs for all the lines, while the rotating-frame magnetization of each line decays exponentially in such an experiment.[8]

Supposing that each atomic jump results in cross relaxation between two different lines in the NMR spectrum, the time evolution of the z magnetization of a selectively saturated line i can be written as

$$m_{z_i} = 1 - \exp\left[-\frac{t}{T_1}\right]\left[\frac{1}{N} + \frac{N-1}{N}\exp(-N\Gamma t)\right], \quad (18)$$

whereas the decay of the z magnetization of all the other lines $j \neq i$ is given by[8]

$$m_{z_j}(t) = 1 - \exp\left[-\frac{t}{T_1}\right]\left[\frac{1}{N} - \frac{1}{N}\exp(-N\Gamma t)\right]. \quad (19)$$

Here, N is the number of lines involved in the atomic jump process and $\Gamma = 1/\tau$ is the mean jump rate. As mentioned above, the rotating-frame magnetization of a selectively locked line i decays exponentially according to

$$m_{\rho_i}(t) = \exp\left[-\left[\frac{1}{T_{1\rho}} + (N-1)\Gamma\right]t\right], \quad (20)$$

where $T_{1\rho}$ denotes the background relaxation time in the rotating frame. A nonselective excitation of the total NMR spectrum leads to the usual exponential decay of each line in both those experiments governed by the background relaxation time T_1 and those governed by $T_{1\rho}$ assumed, respectively, to be of the form

$$m_z(t) = 1 - \exp(-t/T_1), \quad (21a)$$

$$m_\rho(t) = \exp(-t/T_{1\rho}). \quad (21b)$$

Thus, the relaxation of all N lines is assumed to be described by a single relaxation rate. Obviously, the cross relaxation in a site-selective T_1 experiment is a factor of $N/(N-1)$ stronger than in a corresponding $T_{1\rho}$ experiment. This factor has been measured[15] in the case of tellurium, where $N=3$, and was found to be $\frac{3}{2}$. In addition, the nonexponential behavior of the z magnetization leads

to an additional information about the value of N (i.e., the number of lattice sites involved in the atomic jump process). Hence, apart from the simpler realization, a site-selective T_1 experiment offers more sensitive insight into the microscopic details of the atomic jump process than a corresponding $T_{1\rho}$ experiment. Therefore, in the following we will focus only on site-selective T_1 experiments governed by Eqs. (18) and (19).

According to Mehrer's model,[13] in trigonal tellurium and selenium, atomic diffusion occurs via monovacancy-assisted nearest-neighbor (1N) jumps within a chain with an uncorrelated atomic jump rate Γ_1 and next-nearest-neighbor (2N) jumps from chain to chain with an uncorrelated jump rate Γ_2 (1V-1N,2N diffusion model; see also Fig. 1). Within this model the jump frequencies Γ_i ($i=1,2$) must be written as

$$\Gamma_i=\Gamma_{0i}\exp\left[-\frac{E_{1v}+E_{mi}}{kT}\right]=\Gamma_{0i}\exp\left[-\frac{E_i}{kT}\right], \tag{22}$$

where E_{1v} is the energy of monovacancy formation, and E_{mi} and Γ_{0i} denote, respectively, the migration energies and attempt frequencies for 1N and 2N jumps. As illustrated in Fig. 1, each of these jumps goes from an initial lattice site (1) to different lattice sites (2) or (3) (i.e., each jump transfers nuclear magnetization from one line to another). Then, with $i=1$ and $j=2,3$, Eqs. (18) and (19) may be rewritten as

$$m_{z_1}=1-\exp\left[-\frac{t}{T_1}\right]\left[\tfrac{1}{3}+\tfrac{2}{3}\exp(-3\Gamma t)\right] \tag{23}$$

and

$$m_{z_{2,3}}=1-\exp\left[-\frac{t}{T_1}\right]\left[\tfrac{1}{3}-\tfrac{1}{3}\exp(-3\Gamma t)\right], \tag{24}$$

with $\Gamma=\Gamma_1+2\Gamma_2$.

Figure 9 demonstrates clearly the transfer of nuclear magnetization in the ^{77}Se spin system of selenium observed by a selective excitation of line 1. The experiment was performed with the crystallographic X axis being perpendicular to $\vec{H}_0$ (lines 2 and 3 collapse to a single line) and at a temperature of 415 K, where $1/T_1 \ll 3\Gamma$. Then, Eqs. (23) and (24) may be simplified as follows:

$$m_{z_1}\simeq\tfrac{2}{3}[1-\exp(-3\Gamma t)] \tag{25}$$

and

$$m_{z_{2+3}}\simeq\tfrac{2}{3}[2+\exp(-3\Gamma t)]\,. \tag{26}$$

The solid lines in Fig. 9 are smoothed-out time evolutions of the peak intensities of the NMR lines 1 and 2 + 3 following a selective excitation of line 1 and are obtained from Eqs. (25) and (26) with $1/\Gamma=\tau=10.5$ s.

It should be noted that, in principle, the atomic jump rate Γ can be obtained also from an exchange broadening of the NMR lines.[19] Such line broadening becomes remarkable only for $\Gamma>\delta\nu_{1/2}$, while, according to Eqs. (18) and (19), site-selective excitation leads to a pronounced nonexponential behavior if $\Gamma>1/(NT_1)$. Typically, in solids, $NT_1\gg 1/\delta\nu_{1/2}$ (i.e., site-selective experiments are

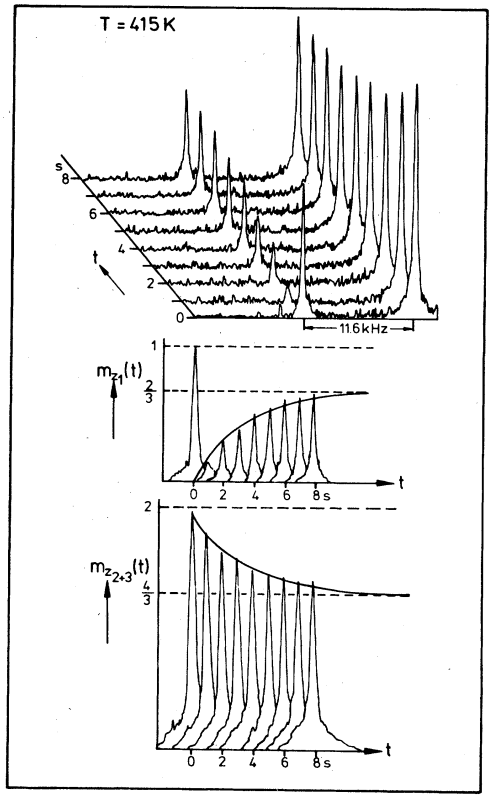

FIG. 9. Transfer of nuclear magnetization between line 1 and line 2,3 of the ^{77}Se spectrum in selenium under site-selective excitation of line 1. In the bottom half, the solid lines are obtained from Eqs. (25) and (26) with an atomic jump rate $\Gamma=0.095$ s^{-1} ($T=415$ K).

a more powerful tool for studying ultraslow motions in solids than exchange broadening). In fact, our measurements have shown that, up to the melting point, the lines of the ^{77}Se spectrum show no observable exchange broadening. In contrast, the widths of the ^{125}Te lines increase strongly with increasing temperature above 550 K. For instance, at $T=650$ K the width is about twice the linewidth at room temperature. Nevertheless, this broadening effect is small compared to the corresponding cross-relaxation effect at $T=650$ K, as can be seen from Fig. 10. This figure shows the temperature dependence of the ^{125}Te Zeeman relaxation rates of line 1 of NMR spectrum (shown in the inset) under selective excitation. The measurements clearly demonstrate the existence of two different relaxation rates, $1/T_1$ and $1/T_1+3\Gamma$, in the time evolution of the nuclear magnetization of line 1 above 470 K, as predicted by Eq. (23). At these temperatures the background relaxation rates given by Eq. (9) are essentially identical at the three nonequivalent lattice sites due to the negligibly small contribution of the orientation-dependent part, $1/T_1\,|_{\rm ph}$ [see Eq. (14)]. Furthermore, it should be noted that, in the temperature range where cross relaxation becomes important, the relaxation rates of line 1 under a uniform excitation of the total spectrum were found to be exactly the same as the T_1 data given by the open circles in Fig. 10. By subtract-

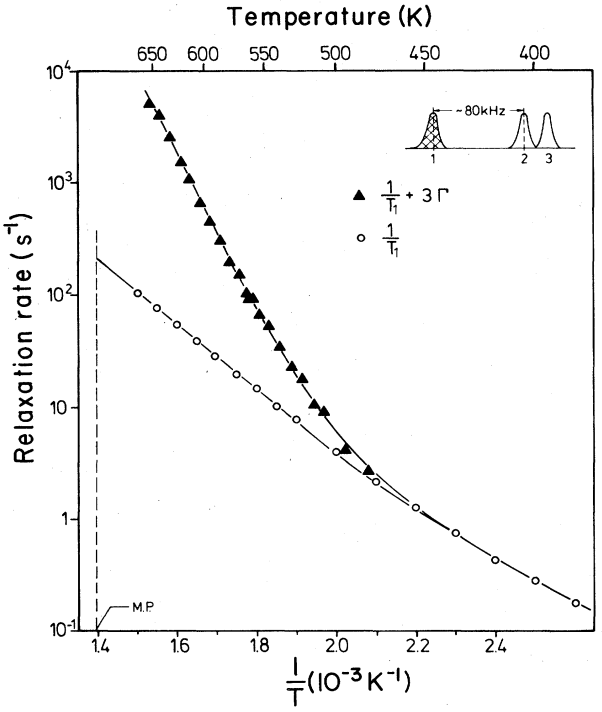

FIG. 10. ^{125}Te nuclear-spin-relaxation rates vs inverse temperature of the selectively excited line 1 in the ^{125}Te spectrum of tellurium, as obtained from the observed evolution of the nuclear magnetization with use of Eq. (23).

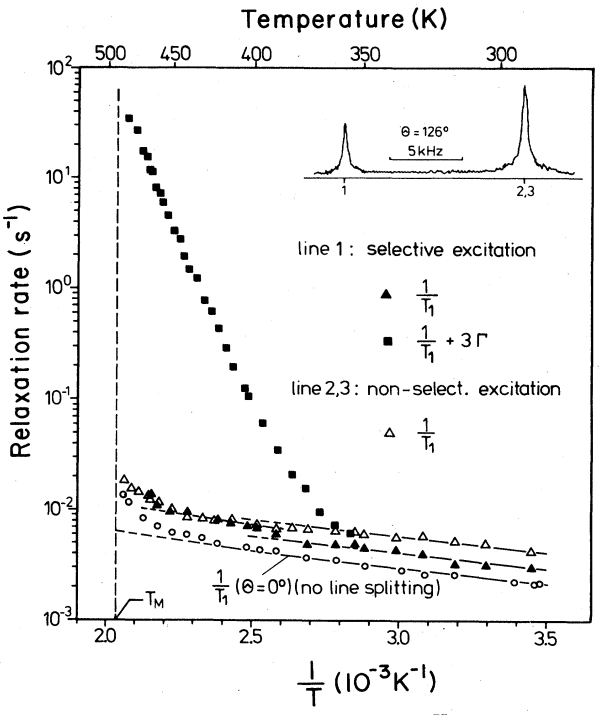

FIG. 11. Temperature dependence of ^{77}Se nuclear-spin-relaxation rates in selenium for different spin excitations. Solid circles: Relaxation rates of the selectively excited line 1 as obtained from the experimental data by means of Eq. (23). Open circles: Relaxation rates $1/T_1$ of line 2+3 (△—△—△) and in a single-line experiment (○—○—○) under a uniform saturation of the spectrum [Eq. (21)].

ing the two rates of Fig. 10, the atomic jump rate $\Gamma=\Gamma_1+2\Gamma_2$ can easily be obtained as a function of temperature.

Analogous to Fig. 10, Fig. 11 shows the ^{77}Se Zeeman relaxation rates in selenium obtained in the different experiments. Again, the solid circles represent the data obtained from selective excitation of line 1 of the NMR spectrum shown in the inset of Fig. 11. Obviously, above 350 K, cross relaxation associated with atomic jumps becomes remarkable and leads to the two different relaxation rates, $1/T_1$ and $1/T_1+3\Gamma$. In addition, nuclear-spin-relaxation rates obtained from nonselective saturation of the NMR spectrum are depicted in Fig. 11. The open triangles illustrate the temperature dependence of the relaxation rate $1/T_1$ of line 2+3, whereas the open circles represent the corresponding relaxation rates $1/T_1$ in the single-line experiment described in the preceding section. Generally, the observed data of these background relaxation rates $1/T_1$ are governed by Eqs. (4) and (14), but show an interesting feature. Above 400 K, the difference between the relaxation rates of line 1 and line 2+3 vanishes and a mean relaxation rate is observed. This phenomenon occurs because the atomic jump rate Γ becomes more rapid than the background rates $1/T_{1i}$ ($i=1,2,3$), resulting in a weighted average of both the relaxation rates of line 1 and line 2+3 as the atoms jump between the two lines. From the experimental data depicted in Fig. 11, the temperature dependence of the atomic jump rate $\Gamma=\Gamma_1+2\Gamma_2$ in selenium can be determined.

V. ATOMIC SELF-DIFFUSION

Mehrer has shown that, within the 1V-1N,2N diffusion model introduced in the preceding section for trigonal tellurium and selenium, the tracer self-diffusion coefficient parallel to the crystallographic c axis is related to the mean atomic jump rate $\Gamma=\Gamma_1+2\Gamma_2$ by

$$D_T^{\parallel}=(c/3)^2(\Gamma_1+2\Gamma_2)f_T^{\parallel}\ , \tag{27}$$

where c is the lattice constant along the c axis. $f_T^{\parallel}$ (with $0\le f_T^{\parallel}\le 1$) denotes the corresponding tracer correlation factor,[13] by which the measured quantity $D_T^{\parallel}$ is smaller than for a random-walk diffusion process. Γ_2 appears in the expression for the macroscopic diffusion coefficient parallel to the crystallographic c axis because the next-nearest-neighbor jumps always have a component parallel to the c axis, as can be seen from Fig. 1. In a similar way, site-selective NMR measurements are also strongly influenced by correlated atomic jump processes. As an example, consider an atom carrying out a series of jumps within a short time interval $\tau\ll\Gamma^{-1}$. Let us further assume that this jump sequence displays the atom from an initial site A_i to a final site A_j, which are both crystallographically equivalent. Such a jump process would contribute to the measured tracer diffusion coefficient, but it does not affect the NMR cross-relaxation behavior after site-selective excitation, because no transfer of nuclear magnetization from one NMR line to another has oc-

curred as a result of this jump sequence. Consequently, the fraction of atomic jump sequences which contribute to the observed cross-relaxation process is given by $1-W_{A\to A}$, where $W_{A\to A}$ denotes the probability for such spatially correlated jump events with equivalent initial and final lattice sites. In addition, the cross-relaxation behavior is also affected by temporal correlations, because a multiple jump process of an atom, occurring within a short time interval $\tau \ll \Gamma^{-1}$, has, in principle, the same effect as a single atomic jump on the time evolution of the selectively excited NMR spectrum. Therefore, the fraction of atomic jumps which influence the NMR cross-relaxation behavior is finally given by $(1-W_{A\to A})/Z$, where Z (≥ 1) denotes the average number of jumps that an atom carries out with a single vacancy. Hence, from site-selective NMR measurements, one does not obtain exactly the uncorrelated atomic jump frequency $\Gamma=\Gamma_1+2\Gamma_2$. Instead, one observes a lower jump frequency Γ_{NMR}, which can be expressed within the 1V-1N,2N diffusion model as

$$\Gamma_{\mathrm{NMR}}=(\Gamma_1+2\Gamma_2)f_{\mathrm{NMR}} , \tag{28}$$

where the correlation factor $f_{\mathrm{NMR}}=(1-W_{A\to A})/Z$ accounts for the spatial as well as the temporal correlation effects described above. In a previous paper we published values of f_{NMR} and of the ratio $f_{\mathrm{NMR}}/f^{\parallel}$, which we obtained as a function of Γ_1/Γ_2 by means of a Monte Carlo simulation of the Γ_1 and Γ_2 jumps.[10] The results can be characterized by only a few features: For $\Gamma_2/\Gamma_1 \gtrsim 0.1$, the ratio $f_{\mathrm{NMR}}/f_T^{\parallel}\simeq 0.9$ is independent of the magnitude of the frequency ratio Γ_2/Γ_1 within a deviation of $\pm 5\%$. The ratio $f_{\mathrm{NMR}}/f_T^{\parallel}$ approaches 1 for Γ_2/Γ_1 approaching zero. For $\Gamma_2/\Gamma_1 \lesssim 0.1$, the correlation factors f_{NMR} and $f_T^{\parallel}$ can be approximated roughly by the same relationship:

$$f_{\mathrm{NMR},T}^{\parallel}\simeq 10\Gamma_2/\Gamma_1 . \tag{29}$$

In order to compare the NMR results (Γ_{NMR}) with radio-tracer measurements ($D_T^{\parallel}$), it is useful to define an NMR diffusion coefficient $D_{\mathrm{NMR}}^{\parallel}$ analogous to Eq. (27) as

$$D_{\mathrm{NMR}}^{\parallel}=(c/3)^2\Gamma_{\mathrm{NMR}} , \tag{30}$$

with Γ_{NMR} given by Eq. (28). From Eqs. (27), (28), and (30) we can draw an important conclusion. If the 1V-1N,2N model is a valid description for the self-diffusion process in tellurium and selenium, then, for all Γ_1/Γ_2 (i.e., for all temperatures), the radio-tracer diffusion along the c axis leads to practically the same diffusion coefficients [Eq. (27)] as those obtained via Eq. (30) by nuclear-spin-relaxation experiments. In the following section diffusion coefficients $D_{\mathrm{NMR}}^{\parallel}$ of tellurium and of selenium, as determined using Eq. (30) from site-selective NMR experiments (Sec. IV B), will be presented and compared with tracer data obtained from the literature.

A. Tellurium

Figure 12 shows a semilogarithmic plot of the dependence of the diffusion coefficients $D_{\mathrm{NMR}}^{\parallel}$ in tellurium on inverse temperature calculated from the experimental data of Fig. 10 by means of Eq. (30). It should be noted that some additional data obtained from site-selective $T_{1\rho}$ experiments are included in the figure. Obviously, in the entire temperature range, the data follow a simple Arrhenius law within the error bars. A least-squares fit (solid line in Fig. 12) yields

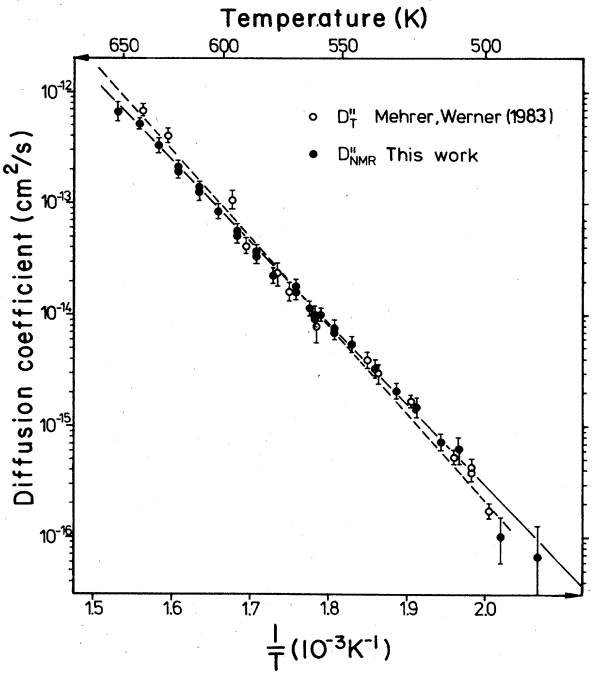

FIG. 12. Self-diffusion coefficients parallel to the c axis, $D^{\parallel}$, vs reciprocal temperature in tellurium single crystals. The solid line represents a least-squares fit of the present NMR data (solid circles) with best-fit parameters given in Eq. (31), while the dashed line is an analogous fit of the radio-tracer data (open circles) as obtained by Werner *et al.* (Ref. 14).

$$D_{\mathrm{NMR}}^{\parallel}=(0.12^{+0.10}_{-0.05})\exp\left[-\frac{(1.45\pm 0.03)\ \mathrm{eV}}{kT}\right] \tag{31a}$$

in units of $\mathrm{cm^2 s^{-1}}$. In addition, self-diffusion coefficients $D_T^{\parallel}$, as obtained recently by Werner *et al.* from ^{127}Te radio-tracer measurements, are depicted in Fig. 12. The dashed line represents a plot of these tracer data using the expression

$$D_T^{\parallel}=(0.6^{+0.8}_{-0.4})\exp\left[-\frac{(1.53\pm 0.04)\ \mathrm{eV}}{kT}\right] \tag{31b}$$

in units of $\mathrm{cm^2 s^{-1}}$. A comparison shows very good agreement within experimental error between these two sets of data, except for a slight deviation above 600 K. Neglecting, for the moment, the three tracer data above 600 K, a least-squares fit of the remaining data leads to an activation energy of 1.43 eV, which is very close to the value given in Eq. (31a). The good agreement of the two sets of data is strong evidence that atomic diffusion in tellurium is dominated by the 1V-1N,2N diffusion mechanism as proposed by Mehrer.[13,29]

In connection with this conclusion, it should be noted that Mehrer *et al.* have also carried out tracer diffusion measurements perpendicular to the crystallographic c axis.[14] They found that through the entire temperature

range the ratio $D_T^{\parallel}/D_T^{\perp}$ lies inside the narrow bounds of $1 \leq D_T^{\parallel}/D_T^{\perp} \leq 1.8$ predicted by the 1V-1N,2N diffusion model.[13] Additionally, their experimental values of $D_T^{\parallel}/D_T^{\perp}$ indicate that $\Gamma_2/\Gamma_1 \lesssim 0.1$ (i.e., atomic mobility is higher along the chains than between the chains). Then, with the use of Eqs. (28) and (29), the diffusion coefficients $D_T^{\parallel}$ [Eq. (27)] and $D_{\mathrm{NMR}}^{\parallel}$ [Eq. (30)] become equal and may be written as

$$D_{\mathrm{NMR},T}^{\parallel} \simeq 10(c/3)^2\Gamma_2(1+2\Gamma_2/\Gamma_1) . \tag{32a}$$

Assuming further, in accordance with Mehrer *et al.*,[14] that both the attempt frequencies Γ_{01} and Γ_{02} in Eq. (22) are equal, we obtain

$$D_{\mathrm{NMR},T}^{\parallel} = D_0 \exp\left[-\frac{E_2}{kT}\right]\left[1+2\exp\left[-\frac{E_{m2}-E_{m1}}{kT}\right]\right], \tag{32b}$$

with $D_0 \simeq 10(c/3)^2\Gamma_{02}$. From the exponential term in the large square brackets of Eq. (32b), we would expect a curvature in the Arrhenius plot of the self-diffusion coefficient (Fig. 12). However, Eq. (32b) predicts a maximum deviation from linear behavior of the Arrhenius plot of only $\pm 6\%$ within the measured temperature range (500–650 K) for $E_{m2}-E_{m1} \simeq 0.07$ eV. For all other positive values of $E_{m2}-E_{m1}$ the nonlinearity is even much less than $\pm 6\%$. On the other hand, the experimental errors of $D_{\mathrm{NMR},T}^{\parallel}$ are larger than about $\pm 10\%$. Therefore, the additional temperature dependence of $D_{\mathrm{NMR},T}^{\parallel}$, introduced by the difference in migration energies for 1N and 2N jumps, cannot measurably influence the temperature dependence of the experimental data. Hence, within the framework of Eq. (32b), the observed effective activation energy of 1.45 eV must be considered the activation energy E_2 for interchain diffusion. We should mention again that this somewhat surprising result is an essential consequence of the correlation effects occurring within the 1V-1N,2N diffusion model under the condition $\Gamma_2/\Gamma_1 \ll 1$ [see Eq. (29)].

B. Selenium

The NMR diffusion data $D_{\mathrm{NMR}}^{\parallel}$ in selenium obtained from site-selective excitation measurements (Fig. 11) by means of Eq. (30) are shown in Fig. 13. Because of the low background relaxation rates in selenium, atomic jump rates Γ_{NMR} could be measured down to about 10^{-4} s^{-1}, corresponding to diffusion coefficients $D_{\mathrm{NMR}}^{\parallel}$ down to about 10^{-19} cm^2/s. In contrast to the diffusion in tellurium, a distinct curvature in the Arrhenius representation of the selenium data is observed, which we interpret in terms of three different diffusion mechanisms:

$$D_{\mathrm{NMR}}^{\parallel} = D_{01}\exp\left[-\frac{E_{\mathrm{eff}}^{\parallel}}{kT}\right] + D_{02}\exp\left[-\frac{E_d}{kT}\right] + D_{03}\exp\left[-\frac{E_3}{kT}\right] . \tag{33}$$

The solid lines in Fig. 13 represent a least-squares fit of the data by means of Eq. (33) using the set of parameters

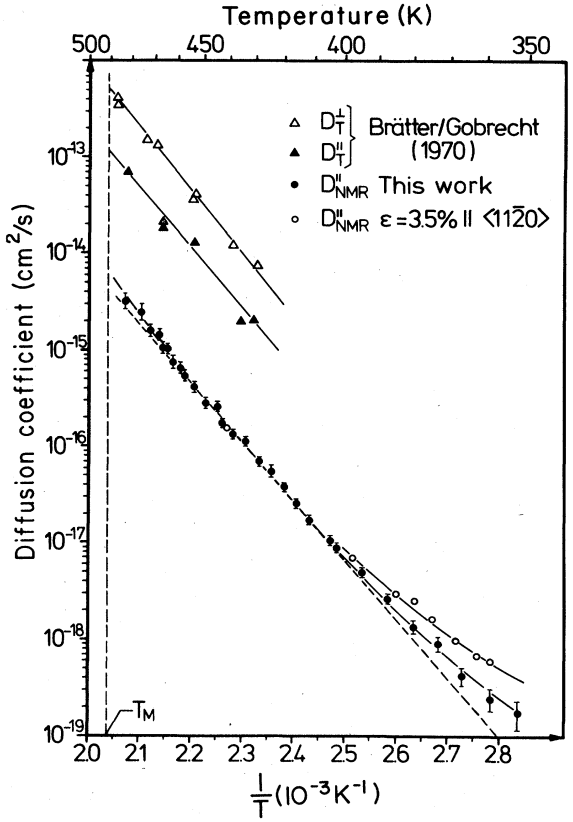

FIG. 13. Arrhenius plot of the self-diffusion coefficient parallel to the c axis, $D_{\mathrm{NMR}}^{\parallel}$, obtained from selective spin excitation in undeformed and plastically deformed ($\epsilon = 3.5\%$) selenium single crystals. The solid lines are computer fits based on Eq. (33); the slope of the dashed line is equal to the activation energy $E_{\mathrm{eff}}^{\parallel} = 1.20$ eV of Eq. (33). For comparison, the tracer diffusion coefficients of Brätter and Gobrecht parallel ($D_T^{\parallel}$) and perpendicular ($D_T^{\perp}$) to the c axis are also shown.

given in Table III. In analogy to isomorphous tellurium, the dominating diffusion process in selenium represented by the first term in Eq. (33) is attributed to the 1V-1N,2N diffusion mechanism introduced by Mehrer.[13] Likewise, we again assume high atomic mobility within the chains (i.e., $\Gamma_2/\Gamma_1 \ll 1$ and $\Gamma_{01} = \Gamma_{02}$), which allows the use of Eq. (32) for the evaluation of the experimental data within the 1V-1N,2N diffusion process. Again neglecting the small temperature dependence of $D_{\mathrm{NMR}}^{\parallel}$ introduced by the difference in migration energies for 1N and 2N jumps [see Eq. (32)], we see that $E_{\mathrm{eff}}^{\parallel}$ represents the activation energy E_2 for interchain atomic diffusion. The dashed line in Fig. 13, which has a slope of 1.20 eV, demonstrates the degree of accuracy of approximating the data by only the first (monovacancy) term in Eq. (33).

The last term in Eq. (33) describes an additional diffusion process in the premelting region ($T > 0.94T_m$). Gilder and Lazarus[30] have proposed that such a contribution may be due to the thermal expansion of relaxed monovacancies, which leads to a temperature dependence of the activation energy and of the preexponential factor D_0. From molecular-dynamics studies in bcc systems Da Fano and Jacucci[31] concluded that the effect may arise

TABLE III. Parameters determining the curvature of the Arrhenius plot of $D^{\parallel}_{\mathrm{NMR}}$ in selenium [see Eq. (33)].

$E^{\parallel}_{\mathrm{eff}}$ (eV)	E_d (eV)	E_3 (eV)	D_{01} (cm^2/s)	D_{02} (cm^2/s)	D_{03} (cm^2/s)
1.20±0.04	0.6±0.2	2.0±0.5	$(8.2^{+15}_{-5})\times10^{-3}$	4.8×10^{-11} ($\epsilon=0\%$) 13×10^{-11} ($\epsilon=3.5\%$)	9×10^{5}

from 1N double jumps of monovacancies which may be thermally activated for $T\gtrsim 0.9T_m$. A third possible explanation of the observed deviation is an additional creation of divacancies at higher temperatures, as proposed by Seeger and Mehrer,[32] resulting in a simultaneous migration of monovacancies and divacancies with different activation energies in that temperature range. The last mechanism seems to be less probable than the first two because of the observed low values of $D^{\parallel}_{\mathrm{NMR}}$. Unfortunately, at the present time, there exists no satisfactory interpretation of the microscopic mechanism of the observed high-temperature contribution.

Obviously, the second term in Eq. (33) is caused by pipe diffusion along dislocations since the corresponding preexponential factor increases with increasing dislocation density ρ produced by a plastic deformation of $\epsilon=3.5\%$ in the $\langle 1120\rangle$ direction, in which the activation energy E_d remains unchanged by the deformation (values given in Table III). Enhanced diffusion along dislocations is generally assumed to occur by a monovacancy mechanism within a vacancy-rich pipe of radius r surrounding the dislocation.[33] Then, the resulting diffusion coefficient D_d can be expressed as

$$D_d = D_{02}\exp\left[-\frac{E_d}{kT}\right] = \pi r^2 \rho D_{0d}\exp\left[-\frac{E_{1v}-E_{v\text{-}d}+E_{md}}{kT}\right], \tag{34}$$

where $E_{v\text{-}d}$ and E_{md} denote, respectively, the mean binding energy and effective migration energy (neglecting the difference between 1N and 2N jumps) of a vacancy near a dislocation.[34] From the nuclear-spin-relaxation point of view, one requires within this model that a common spin temperature is established after each atomic jump inside the dislocation pipe [i.e., the spin diffusion coefficient D_s must be large compared to the atomic diffusion coefficient $D^{\parallel}_{\mathrm{NMR}}$, which is of the order of 10^{-18} cm^2/s (see Fig. 13)]. The spin diffusion coefficient D_s is related to the dipolar local field $\omega_D\simeq\pi\nu_D$ according to $D_s\simeq(c/3)^2\omega_D/10$ (Ref. 35). Hence, from Eq. (30), $D_s/D^{\parallel}_{\mathrm{NMR}}\sim\nu_D/\Gamma$. For ^{77}Se in selenium, $\nu_D\sim10^2$ Hz and $\Gamma(370\ \mathrm{K})\sim10^{-3}$ s^{-1} (Fig. 11), and obviously, the condition $\nu_D/\Gamma\gg1$ is fulfilled.

Suppose that the attempt frequencies Γ_{0i} do not change around a dislocation. Then $D_{0d}=D_{01}$, or $D_{02}/D_{01}=\pi r^2\rho$. Taking a pipe radius r of about 5×10^{-8} cm, commonly assumed to be realistic in nonionic solids,[36] a typical dislocation density ρ of nearly 10^6 cm^{-2} leads to $\pi r^2\rho\simeq10^{-8}$, which is indeed of the same order of magnitude as the ratios D_{02}/D_{01} obtained from the data in Table III. Values of $E_{v\text{-}d}$ and E_{md} in Eq. (34) have never been measured directly, but estimates may be obtained from the experimental data. As discussed above, for $\Gamma_2/\Gamma_1\ll1$, the energy $E^{\parallel}_{\mathrm{eff}}$ was found to be equal to $E_2=E_{1v}+E_{m2}$. Then, with Eq. (34), the difference $E^{\parallel}_{\mathrm{eff}}-E_d=0.6$ eV is equal to $E_{m2}+E_{v\text{-}d}-E_{md}$. Peterson[37] argued that the energies to form and to move vacancies in dislocations are about 0.5 of the corresponding values in the lattice (i.e., $E_{md}\simeq0.5E_{m2}$). Furthermore, Stuke[38] has studied the recovery of selenium single crystals after plastic deformation as a function of temperature. He concluded that the annealing occurs via motion of vacancies with a migration energy of about 0.6 eV. Together, these data lead to a binding energy $E_{v\text{-}d}$ for a vacancy in the dislocation pipe of about 0.3 eV, which seems to be in acceptable agreement with the theoretical background of pipe diffusion.[37]

For comparison, self-diffusion coefficients $D^{\parallel}_T$ and $D^{\perp}_T$ obtained by Brätter and Gobrecht from ^{75}Se radio-tracer measurements[12] are depicted in Fig. 13. Obviously, the data lead roughly to the same activation energy as that measured by nuclear spin relaxation, but the absolute values of the diffusion coefficients differ by a factor of the order of 20. The reason for the discrepancy is not completely clear. In our opinion the tracer data are probably influenced by lattice imperfections caused by the preparation technique of the samples. The anomalous behavior of the penetration profiles published by Brätter and Gobrecht may support such an assumption. Similarly, Werner *et al.*[14] have observed a similar discrepancy in self-diffusion in tellurium by comparing their own tracer data (depicted in Fig. 12) with previous tracer measurements performed on tellurium crystals of reasonable quality, as described in the literature.[11] They concluded that lattice defects, like dislocations, are probably the source of the higher diffusivities published by Ghoshtagore.[11] On the other hand, as discussed in the preceding section, their diffusion coefficients exhibit excellent agreement with the present results of site-selective excitation experiments carried out on the same tellurium crystals. Hence, these results suggest that, in particular, in tellurium and in homologous selenium self-diffusion is significantly enhanced by lattice distortions. However, it remains difficult to explain that in both materials only the preexponential factor is substantially affected, whereas the activation energy (i.e., the slope of the Arrhenius plots) remains nearly unchanged.

ACKNOWLEDGMENTS

We appreciate many helpful discussions with Dr. D. Wolf, Professor H. Mehrer, and Dr. N. Peterson, and a critical reading of the manuscript by Professor D. Ailion. We kindly thank Dr. H. Siethoff and Professor D. Fröhlich for providing the tellurium and selenium single crystals, respectively, used in this research.

[1]P. Grosse, *Die Festkörpereigenschaften von Tellur,* Vol. 48 of *Springer Tracts in Modern Physics,* edited by G. Hohler (Springer, New York, 1969).
[2]A. Koma and S. Tanaka, Solid State Commun. **10**, 823 (1972).
[3]A. Koma, Phys. Status Solidi B **56**, 655 (1973).
[4]M. Bensoussan, J. Phys. Chem. Solids **28**, 1533 (1967).
[5]M. Bensoussan, J. Phys. Chem. Solids **35**, 1661 (1974).
[6]H. Selbach, O. Kanert, and D. Wolf, Phys. Rev. B **19**, 4435 (1979).
[7]A. Koma, A. Hajo, and S. Tanaka, Phys. Lett. **28A**, 95 (1968).
[8]O. Kanert, Phys. Rep. **91**, 185 (1982).
[9]O. Kanert, R. Küchler, and J. Recktenwald, Solid State Commun. **33**, 993 (1980).
[10]B. Günther, O. Kanert, and D. Wolf, Solid State Commun. **47**, 409 (1983).
[11]R. N. Ghoshtagore, Phys. Rev. **155**, 598 (1967).
[12]O. Brätter and H. Gobrecht, Phys. Status Solidi **37**, 869 (1970).
[13]H. Mehrer, J. Phys. C **15**, 1637 (1982).
[14]M. Werner, H. Mehrer, and H. Siethoff, J. Phys. C **16**, 6185 (1983).
[15]B. Günther, O. Kanert, M. Mehring, and D. Wolf, Phys. Rev. B **23**, 6747 (1981).
[16]J. Henning and H. H. Limbach, J. Magn. Reson. **49**, 322 (1982).
[17]J. J. Led and H. Gesmar, J. Magn. Reson. **49**, 444 (1982).
[18]J. Schotland and J. S. Leigh, J. Magn. Reson. **51**, 48 (1983).
[19]A. Abragm, *The Principles of Nuclear Magnetism* (Clarendon, Oxford, 1961).
[20]J. H. Van Vleck, Phys. Rev. **74**, 1168 (1948).
[21]C. Kittel and E. Abrahams, Phys. Rev. **90**, 238 (1953).
[22]W. Hörstel and G. Kretschmar, Phys. Status Solidi **23**, 639 (1967).
[23]B. Günther, Ph.D. thesis, University of Dortmund, 1983 (unpublished).
[24]A. Abragam and B. Bleany, *Electron Paramagnetic Resonance of Transition Ions* (Clarendon, Oxford, 1970).
[25]Yu. V. Kosichkin, in *The Physics of Selenium and Tellurium,* Vol. 13 of *Springer Series in Solid State Sciences,* edited by E. Gerlach and P. Grosse (Springer, Berlin, 1979), pp. 96—109.
[26]H. C. Torrey, Phys. Rev. **92**, 962 (1953).
[27]D. Wolf, *Spin Temperature and Nuclear Spin Relaxation in Matter* (Clarendon, Oxford, 1979).
[28]C. A. Sholl and W. A. Barton, J. Phys. C **9**, 4315 (1976).
[29]H. Mehrer (private communication).
[30]M. Gilder and D. Lazarus, Phys. Rev. B **11**, 4916 (1975).
[31]A. Da Fano and G. Jacucci, Phys. Lett. **39**, 950 (1977).
[32]A. Seeger and H. Mehrer, in *Vacancies and Interstitials in Metals,* edited by A. Seeger, D. Schumacher, W. Schilling, and J. Diel (North-Holland, Amsterdam, 1970).
[33]R. W. Baluffi, Phys. Status Solidi **42**, 11 (1970).
[34]A. Atkinson and R. I. Taylor, Philos. Mag. A **39**, 581 (1979).
[35]N. Bloembergen, Physica (Utrecht) **15**, 386 (1949); A. G. Redfield and W. N. Yu, Phys. Rev. **169**, 443 (1968).
[36]A. D. Le Claire and A. Rabinovitch, J. Phys. C **14**, 3863 (1981).
[37]N. L. Peterson, Int. Metall. Rev. **28**, 65 (1983), and private communication.
[38]J. Stuke, Phys. Status Solidi **6**, 441 (1964).